Brodogradnja/Shipbuilding/Open access Volume 73 Number 2, 2022

Ali Dogrul

http://dx.doi.org/10.21278/brod73202

ISSN 0007-215X
eISSN 1845-5859

NUMERICAL PREDICTION OF SCALE EFFECTS ON THE PROPULSION PERFORMANCE OF JOUBERT BB2 SUBMARINE

UDC 629.585:629.5.016
Original scientific paper

Summary

The motivation of this study is to present the scale effects on the propulsion performance of Joubert BB2 submarine with MARIN7371R propeller. Joubert BB2 submarine was designed as a realistic attack submarine to be used in benchmarking studies. Numerical analyses were conducted solving RANS equations. The propeller in the self-propelled case was modeled using the body force method. The numerical method was verified both for submarine and open water propeller cases. The resistance, open water propeller and propulsion characteristics were validated with the available numerical/experimental data. After, the results were extrapolated to the full-scale and compared with other studies. Full-scale RANS analyses were then conducted to calculate the resistance and propulsion parameters by eliminating the possible scale effects. The extrapolated full-scale results were compared with the full-scale analyses and self-propulsion method (SPE) results. The scale effects on the resistance and propulsion parameters were obtained in detail. 1978 ITTC prediction method coupled with the body force method was utilized to observe the scale effects. In addition to this, the practicality of the SPE method for the estimation of the propulsive performance was shown. The scale effects on the propulsive parameters such as nominal wake and thrust deduction factors, open water propeller efficiency and propulsion efficiency were seen.

Key words: *Body force; CFD; Joubert BB2; MARIN 7371R; Self-propulsion*

1. Introduction

Hydrodynamic research on ships has been an important and actual issue for over a century. The hydrodynamic performance of ships has a significant effect on other topics such as hydroacoustics and structural strength. Within this aspect, various experimental and numerical methods have been widely used to determine the hydrodynamic characteristics of surface and submerged vessels. However, most of the studies are based on the surface vessels' behavior. Several benchmark geometries (container ships, tankers, bulk carriers, planing hulls) have been developed and tested/analyzed in terms of calm water resistance and self-propulsion, seakeeping and maneuvering. When it comes to submerged vessels, it is obvious that the studies are few when compared with the surface vessels. However, it is very important to estimate the submarine hydrodynamics with good precision and accuracy. For this purpose, validation

studies should be made using benchmark submarine models. Only two benchmark models (DARPA Suboff, Joubert BB2) are available to be investigated by the researchers. DARPA Suboff geometries including the bare and appended hulls are already being studied in various model scales including the full-scale. Joubert BB2 submarine model is also studied but the studies are focused on the maneuvering performance and self-propulsion performance during maneuvering. In other words, there are few studies of Joubert BB2 for calm water resistance and self-propulsion. In the meantime, this submarine was designed as a realistic attack submarine (SSK) having two variants (BB1 and BB2) despite the DARPA Suboff model. Therefore, most of the studies about submarine hydrodynamics are focused on the DARPA form while there are very few studies regarding the Joubert form.

In thesis work by Chase [1] and another study by Chase and Carrica [2], the authors examined the effects of various turbulence models on the self-propulsion hydrodynamics of the DARPA Suboff model with the E1619 propeller model. The wake velocities of different turbulence models and model experiments were compared in detail. The paper of Sezen et al. (Sezen et al., 2018) involves a comprehensive study on the self-propulsion of DARPA Suboff generic submarine with E1619 in model scale. Virtual disk model and discretized rotating propeller model were used for the propulsion analyses and its characteristics were obtained in a wide range of velocities. These two models were discussed in detail and it is concluded the virtual disk model estimates the delivered power higher than the actual propeller. Kinaci et al. [3] investigated the surface vessels DTC and KCS, a generic submarine model (DARPA Suboff) numerically to determine the self-propulsion characteristics. The numerical results were obtained using different methods and compared with the available experimental data. The study of Posa et al. [4] deals with the LES analyses of the DARPA Suboff submarine model. Resistance and self-propulsion analyses were made to examine the velocity and vorticity fields around the hull and E1619 model propeller. Takahashi and Sahoo conducted a numerical study for DARPA Suboff with discretized E1619 propeller and the self-propulsion performance was determined. Detailed uncertainty analysis was made and the results were discussed in terms of self-propulsion point. Ozden et al. [5] performed a validation study for DARPA Suboff generic submarine model. The numerical analyses were conducted using a discretized rotating propeller model of E1619 and the results were compared with the model tests by means of total resistance, propeller revolution, thrust deduction, wake fraction and propulsive efficiencies. In another study, Wang et al. [6] focused on the investigation of the flow around DARPA Suboff with E1658 model propeller. Model experiments and numerical analyses were conducted considering the free surface effects in different depths. The nominal wake behind the submarine and the vertical structures around the propeller blades were examined in detail. In another recent study, Sezen et al. [7] conducted numerical analyses in different scales including the full-scale for DARPA Suboff AFF-8 geometry. The scale effects on the resistance components and self-propulsion characteristics were observed. Also, the 1978 ITTC prediction method was used for the full-scale extrapolation and the results were compared with the full-scale CFD results. The results showed that the prediction method can be used for the submerged bodies.

Overpelt et al. [8] investigated the flow around a 4000t attack submarine in submerged and surfaced conditions. Joubert BB1 design was used and different bow shapes were generated to observe the change in wave-making resistance. The model experiments were conducted and the results were compared for different conditions and bow shapes. Finally, the full-scale resistance and power were predicted. In another form optimization study, Toxopeus et al. [9] dealt with the junction flow phenomenon for the Joubert BB1 submarine. The sail fin geometry that causes the junction flow was investigated by generating different sail fins with NACA sections. The effect of sail fin thickness on the flow was observed numerically. Each fin configuration was verified with an uncertainty assessment and the results were compared using the wake object function. It is concluded that the thinner sail fin located near the nose creates

less resistance. In another paper by Overpelt et al. [10], the BB2 submarine was investigated experimentally for the observation of submerged maneuvering performance. A stock propeller MARIN 7371R was chosen as the propulsion unit and the towing tests were conducted in model scale. Horizontal and vertical plane maneuvers were simulated and a comprehensive data set was presented including zigzag, roll decay tests, turning circle and the effectiveness of sail and stern planes. Carrica et al. [11] employed various numerical solvers for grid generation and flow simulation around the Joubert BB2 submarine. Self-propulsion and maneuvering analyses were conducted and the results were presented in full-scale. Self-propulsion analyses were made at 10 knots for the submerged condition while the near-free surface condition was analyzed at various velocities. Maneuvering analyses were made at 10 and 12 knots to obtain zigzag maneuvering data. Hally [12] focused on the calculation of effective wake for BB2 submarine. The body force method based on a BEM solver was employed to reduce the computational cost. The numerical results of BEM were compared in terms of axial, radial and tangential velocities. After that, RANS-BEM coupling was made and the interaction between BB2 submarine and MARIN 7371R six-bladed propeller was modeled. The results were compared with the experimental ones at one ship velocity. Pontarelli [13] and Pontarelli et al. [14] investigated the propeller crashback phenomenon. DTMB4381 and MARIN7371R propellers were investigated numerically at various advance coefficients in open water conditions. Axial and side forces acting on the propellers were obtained for negative and positive advance coefficients simulating the crashback problem. After, the MARIN7371R propeller was modeled behind Joubert BB2 submarine and the instabilities in the flow field were observed in case of a crashback maneuver. In a thesis work, Kim [15] investigated the maneuvering performance of the Joubert BB2 submarine numerically. First, a reliable CFD methodology was developed in forward motion using DARPA Suboff AFF-1 and AFF-8 submarines. This methodology was employed for BB2 geometry and captive self-propulsion analyses were conducted. After, free-running analyses were performed using an actuator disk based on the body force method instead of a discretized propeller. The numerical analyses were validated with the experimental ones. The results were found in good agreement in terms of turning radius, tactical diameter and transfer distance. Kim et al. [16] analyzed the attack submarine Joubert BB2 numerically with the six-bladed propeller MARIN7371R. The effect of flow angle was investigated. The model propeller was modeled in open water condition at various angles. Following this, the submarine with the discretized propeller was modeled at the same angles. The results were discussed for the velocity distributions and it is concluded that the incidence flow angle affects the propeller loading significantly. In the study of Carrica et al. [17], the generic submarine Joubert BB2 was chosen for the numerical investigation of self-propulsion performance. The numerical analyses were carried out considering the submarine moving near the free surface in calm water and regular wave conditions. The authors concluded that the interaction between the hull and free surface causes fluctuations in the wake and propeller thrust. In another study, Carrica et al. [18] investigated the vertical zigzag maneuvering performance of the Joubert BB2 submarine numerically. Different grid topologies including moving reference frame and rotating propeller were used. The self-propelled captive model was analyzed and compared with the experimental data. After, the maneuvering simulations were conducted in model and full-scale. It is concluded that the motion responses were good in model scale when compared to full-scale. However, the forces and moments were strongly affected by the scale. In another numerical study, maneuvering analyses of the Joubert BB2 submarine were conducted for the X-plane rudder configuration by Cho et al. [19]. A verification study was made for the captive model in terms of total resistance. Pure sway, pure yaw, pure heave and pure pitch simulations were carried out. Turning circle test was made and the tactical diameter value was found similar to the experimental data.

Thus far, the recent literature was searched especially focusing on submarine hydrodynamics. To the best of the author's knowledge, few full-scale numerical studies are related to the DARPA Suboff geometry. The resistance data is available for BB1 design while the geometry is not shared for academic use. And BB2 geometry is shared while there is a lack of experimental/numerical data in terms of resistance and self-propulsion characteristics. The available and very limited resistance and self-propulsion data for BB2 are the extrapolated full-scale results and full-scale CFD results at a narrow velocity range.

This study aims to give comprehensive total resistance and self-propulsion performance data in model and full scale. The numerical analyses were carried out using a viscous solver solving RANS equations. The flow around Joubert BB2 was simulated to obtain the velocity-total resistance curve. Following this, the open water performance of the MARIN7371R propeller was calculated. Self-propulsion characteristics of the Joubert BB2 submarine with MARIN7371R propeller were predicted using the body force method. Within this approach, the open water curve of the propeller was implemented into an actuator disc located behind the submarine hull. The total resistance and open water propeller analyses were verified using various uncertainty methods. Following this, the numerical analyses were extended to a wide range of ship velocities both for total resistance and propulsion estimation. The validation study was made by comparing the numerical results with the available experimental/numerical data. The propulsion data was also compared with the self-propulsion estimation (SPE) method in terms of various propulsive parameters. The full-scale results were obtained by using the 1978 ITTC prediction method. Full-scale extrapolated results were compared with similar full-scale results since there is a lack of any sea trial data. Again, the full-scale results were compared with the SPE method. Finally, full-scale RANS analyses were carried out and all results were compared with the full-scale CFD results. Scale effects on the propulsive parameters were discussed in detail.

This paper is organized as follows: Section 1 is giving a brief literature review. Section 2 is for the main particulars of the submarine and propeller geometries while Section 3 is for the methodology applied in this study. Section 4 presents the uncertainty assessment and gives the numerical verification results. The numerical results for resistance and open water analyses were given in Section 5 while Section 6 presents the self-propulsion results in model and full scale. The results were discussed in Section 7. Finally, conclusions were presented in Section 8.

2. Submarine and Propeller Geometries

The most popular benchmark submerged vessel is the DARPA Suboff design. In addition to this, a more realistic SSK class attack submarine design was proposed by Joubert [20,21]. Joubert BB1 submarine model was used for the prediction of total resistance at submerged and surfaced conditions. In this study, the BB2 variant of the submarine was used to predict the total resistance and propulsive parameters numerically. Table 1 shows the 3-D model and main particulars of the Joubert BB2 submarine. The BB2 model was developed by Maritime Research Institute Netherlands (MARIN) originating from the BB1 model. Table 2 shows the 3-D model and main particulars of the propeller. The six-bladed propeller 7371R was designed by Maritime Research Institute Netherlands (MARIN). 3-D models of the submarine and the propeller can be seen in Figure 1.

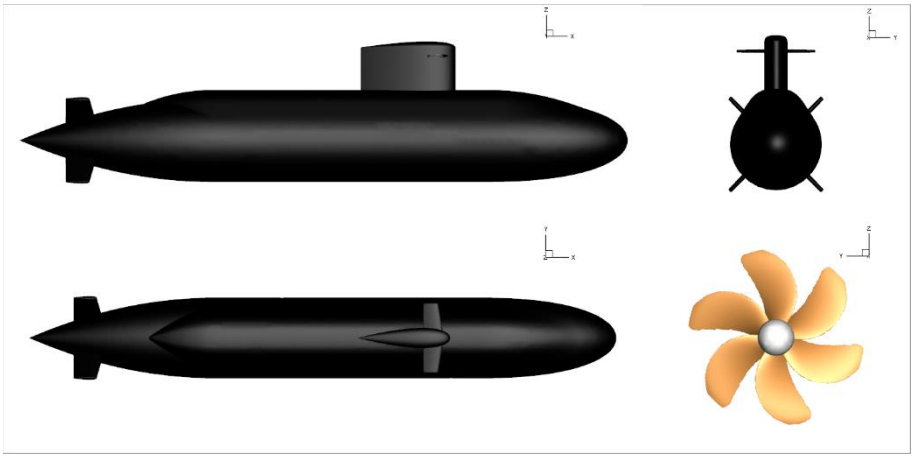

Fig. 1 3-D models of the submarine and the propeller

Table 1 Main particulars of Joubert BB2

Designation	Description	Model	Full
λ	Scale factor	18.348	1
L_{OA} (m)	Length	3.8260	70.2
B (m)	Beam	0.5232	9.6
D_d (m)	Draught to deck	0.5777	10.6
D_s (m)	Draught to sail top	0.8829	16.2
WSA (m^2)	Wetted surface area	6.4455	2169.91
Δ (ton)	Displacement	0.7012	4440

Table 2 Main particulars of MARIN 7371R

Designation	Description	Model	Full
λ	Scale factor	18.348	1
D (m)	Diameter	0.272	5.0
P/D	Pitch ratio	0.966	
Z	Number of blades	6	
D_h/D	Hub diameter ratio	0.175	
A_E/A_0	Expanded area ratio	0.740	
Rotation	-	Right-handed	

3. Numerical Approach

3.1 Theoretical Background

The numerical analyses were conducted using a commercial CFD software, Siemens PLM STAR CCM+, solving Reynolds-Averaged Navier-Stokes (URANS) equations. The governing equations are the continuity equation and the momentum equations considering the flow is incompressible and turbulent. The continuity equation can be given as:

$$\frac{\partial U_i}{\partial x_i} = 0 \tag{1}$$

The mean momentum equations can be written in tensor notation and Cartesian coordinates.

$$\frac{\partial U_i}{\partial t}+U_j\frac{\partial U_i}{\partial x_j}=-\frac{1}{\rho}\frac{\partial P}{\partial x_i}+\frac{\partial}{\partial x_j}\left[\upsilon\left(\frac{\partial U_i}{\partial x_j}+\frac{\partial U_j}{\partial x_i}\right)\right]-\frac{\partial\overline{u_i^{'}u_j^{'}}}{\partial x_j} \tag{2}$$

Here, ρ depicts the fluid density, kg/m^3; U_i is the velocity, m/s; P represents the pressure, Pa; υ is the kinematic viscosity, m^2/s. The last two terms belong to the viscous stress tensor and Reynolds stress tensor, respectively. The details about Reynolds stress tensor (i.e., ($\overline{u_i^{'}u_j^{'}}$) and the turbulence model (k-ω SST) can be found in Wilcox in detail [22,23].

3.2 Computational Domain, Boundary Conditions and Grid Structure

The computational domain with appropriate boundary conditions was created around the submarine model and the propeller model separately as given in Figure 2. The domain dimensions for the resistance and self-propulsion analyses were selected following the ITTC guideline [24]. The upstream and the downstream of the domain were extended 2L_{PP} and 5L_{PP}, respectively. The distance between the top/bottom surfaces and the submarine centerline was set to 2.5L_{PP}. The total width of the domain was also set to 5L_{PP}. The outer domain diameter for the open water propeller flow was set to 14D while the inner domain diameter is 1.5D. The downstream and the upstream of the domain were extended 12D and 5D, respectively. Here, the outer domain is the static region and the inner domain is to be the rotating region. The inlet surface in both submarine and propeller analyses was defined as velocity inlet to apply a uniform inflow velocity. The outlet surface is defined as pressure outlet. In both analyses, the body surfaces (e.g. submarine hull and its appendages, propeller blades and its shaft) were set as no-slip wall. The remaining surfaces were set as symmetry plane which dictates that the normal component of the velocity is zero on these surfaces.

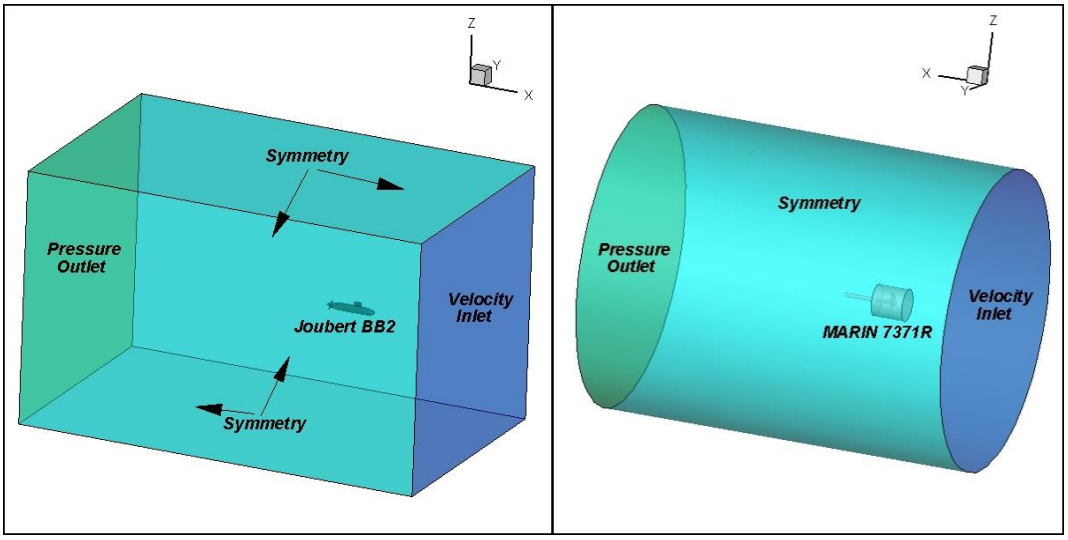

Fig. 2 Boundary conditions for the submarine and the propeller

As given in Figure 3, mostly hexahedral elements were employed on the submarine surfaces and the whole computational domain. Trimmer mesh algorithm was used and the domain was discretized with finite hexahedral volume elements. The prism layer approach was also used to model the boundary layer and near-wall flow field. Wall functions implemented in the turbulence model were employed and appropriate wall y^+ distributions ($30<y^+<300$) were obtained in each submarine velocity, which is identical to the ITTC guideline [24]. Figure 4

shows an example of the wall y^+ distribution on the submarine hull at 10 knots. The average wall y^+ value on the submarine surfaces was calculated between 55 and 215 for all inflow velocities. Average wall y^+ values on the propeller blades were also calculated between 40 and 100 for all advance coefficients in open water conditions. The average wall y^+ values on the submarine surfaces were kept between 500 and 600 as consistent with similar studies [7,25,26].

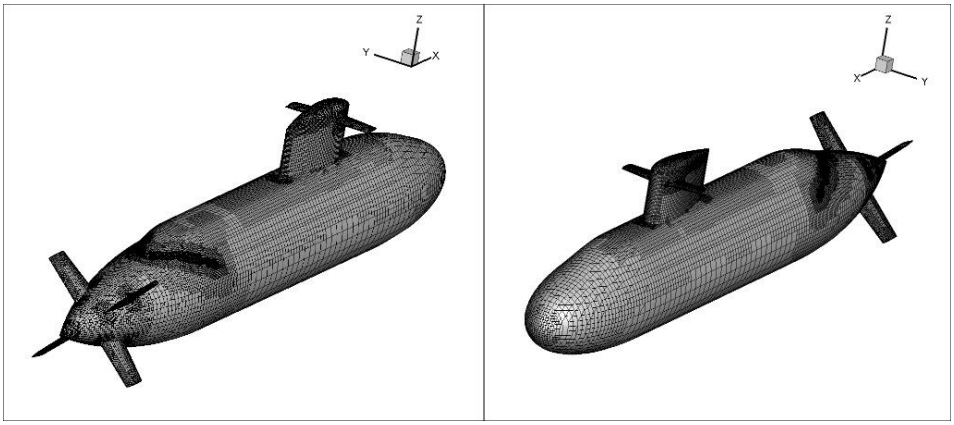

Fig.3 Grid structure on the submarine hull

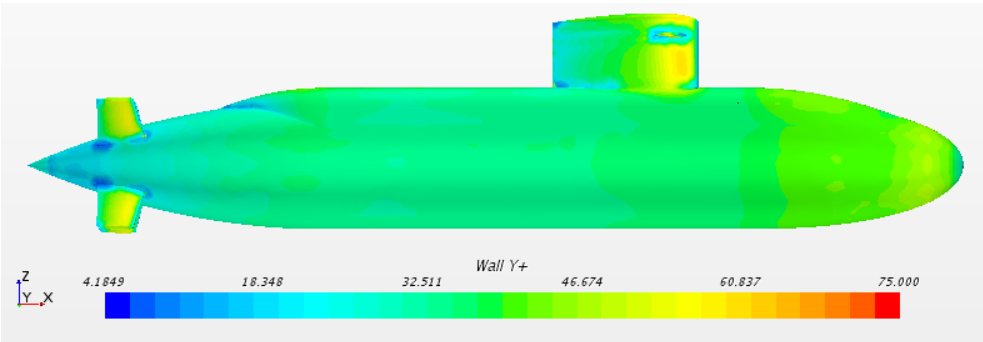

Fig. 4 Wall y^+ distribution on the submarine hull in model scale at 10 knots

3.3 Physics Modelling

The numerical analyses were conducted using the commercial CFD software package STAR-CCM+. The resistance and self-propulsion analyses were done considering the submarine is submerged, hence free surface effects were neglected in this study. The solution procedure for the governing equations was based on the Semi-Implicit Method for Pressure-Linked Equations (SIMPLE) type algorithm that calculates the pressure and velocity fields in an iterative manner. The flow was modeled using the k-ω SST (Shear Stress Transport) turbulence model. This model uses the k-ω formulation inside the boundary layer and k-ε formulation in the free-stream using all wall y^+ treatment. This approach ensures a more accurate near-wall treatment and a better prediction of adverse pressure gradients caused by the separating flow [27–29].

The open water propeller analyses were conducted using the Moving Reference frame (MRF) method. This method transforms the governing equations into a rotating frame to get a steady-state solution [30]. It also provides less computational cost when compared with the Rigid Body Motion (RBM) method. Since the main aim of the open water analyses is to obtain the thrust and torque values that have a steady-state behavior, the analyses were done steadily as used in recent studies [7,31].

The numerical analyses for propulsion were conducted using the same mesh structure and numerical model of the total resistance analyses. In addition, an actuator disc was created on

the propeller plane to mimic the propeller instead of a computationally demanding rotating propeller. Thus, the surface mesh on the submarine was not changed, so the wall y^+ values were kept constant. An additional mesh refinement was employed for a better grid generation behind the submarine focusing on the propeller plane and downstream.

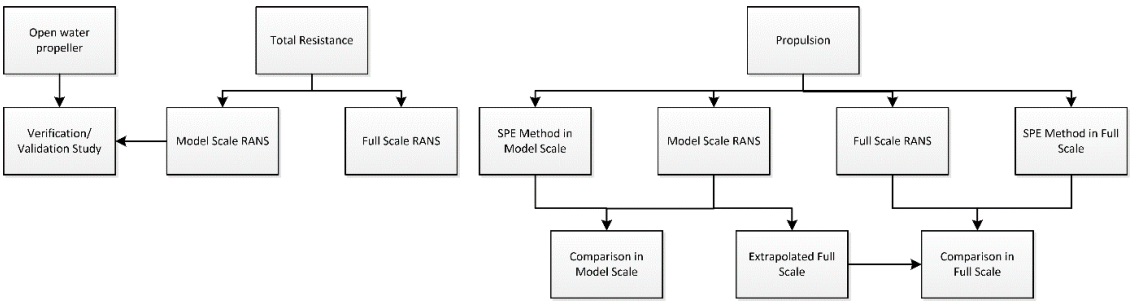

Fig. 5 The methodology followed in this study

4. Numerical Uncertainty

For the uncertainty assessment of the numerical method, a verification study was carried out by means of grid size. Fine, medium and coarse grid sizes are used to create different grid numbers to calculate the spatial uncertainty. The verification study was made for the submarine model at a constant velocity (10 knots) and for the propeller model at a constant advance coefficient (J=0.7). The numerical uncertainty originating from the spatial discretization was estimated using the Grid Convergence Index (GCI) method [32] and Correction Factor method (CF) [33], as used by recent numerical studies [31,34–36]. GCI method is recommended by the ITTC guideline about the uncertainty in the ship resistance calculations [37] while ASME [32] and AIAA [38] also recommend this method in several application areas. Details of the GCI method, two different variants of the GCI method and the Correction Factor (CF) method can be found in Xing and Stern [33]. $\varphi_1, \varphi_2, \varphi_3$ indicate the fine, medium, and coarse grid solution, respectively. The solution scalar here was the total resistance of the submarine and the non-dimensional thrust coefficient of the propeller.

Table 3 Spatial uncertainty parameters for the model submarine and model propeller

Parameter	$R_T(N)$ (Joubert BB2)	K_T (MARIN 7371R)
N_1	737206	3456744
N_2	525596	1997746
N_3	377815	1239052
φ_1	20.244	0.16110
φ_2	20.506	0.16056
φ_3	21.083	0.15238
$\%U_{GCI}$	1,28044	0,0249
$\%U_{GCI1}$	0,25642	0,00065
$\%U_{GCI2}$	0,61541	0,00157
$\%U_{CF}$	2,66277	2,2798

The numerical uncertainty in terms of spatial discretization was calculated using three different GCI methods and the CF method. Table 3 shows the uncertainty parameters for the model submarine and propeller. Here, N_i stands for the total grid number. The scalar functions (φ_i) in the calculations were considered as the total resistance for the model submarine at 10 knots and the non-dimensional thrust coefficient for the model propeller at J=0.7. Both analysis sets have a monotonic convergence [39] ($0 < R < 1$). The most conservative method is the Correction Factor (CF) method having a higher FS (Factors of Safety) constant. In consideration of these results, the fine grid was used for the total resistance and self-propulsion analyses. Medium grid was selected for the open water propeller analyses since the relative difference between the fine and medium grids is too low.

5. Resistance and Open Water Analyses

5.1 Propeller Open Water Analysis

The model propeller MARIN 7371R was analyzed in open water conditions numerically. The propeller was modeled and the open water curves were obtained at various advance coefficients. The numerical results were compared with another study [14] and found in good agreement. The difference between the two results decreases with the increase in the advance coefficient. The open water performance data is crucial to observe the self-propulsion performance using the body force method. These curves are the input to be applied in the actuator disc located at the propeller plane behind the submarine hull for the appropriate representation of the propeller. The open water curves are also used in the determination of the self-propulsion characteristics using the thrust-identity method. The non-dimensional coefficients in Figure 6 are calculated by the following equations.

$$J = \frac{V_A}{nD} \tag{3}$$

$$K_T = \frac{T}{\rho n^2 D^4} \tag{4}$$

$$K_Q = \frac{Q}{\rho n^2 D^5} \tag{5}$$

$$\eta_0 = \frac{J}{2\pi}\frac{K_T}{K_Q} \tag{6}$$

Here, $n(rps)$ is the rate of revolution per second, D (m) is the propeller diameter and V_A (m/s) is the average advance velocity in the axial direction at the propeller plane. T (N) is the thrust force and Q (Nm) is the torque obtained from the propeller blades. η_0 is the open water propeller efficiency. The thrust coefficient was found very close to the other results [14] while there is some difference in the torque coefficient. This may be caused by the turbulence model used in the study. The present study uses the k-ω SST turbulence model while the other study employs DDES (Delayed Detached Eddy Simulation) model. In the DDES model, a very high number of grid is generated around the propeller blades and blade tips to model the tip vorticities precisely. This may cause a difference in the torque coefficient.

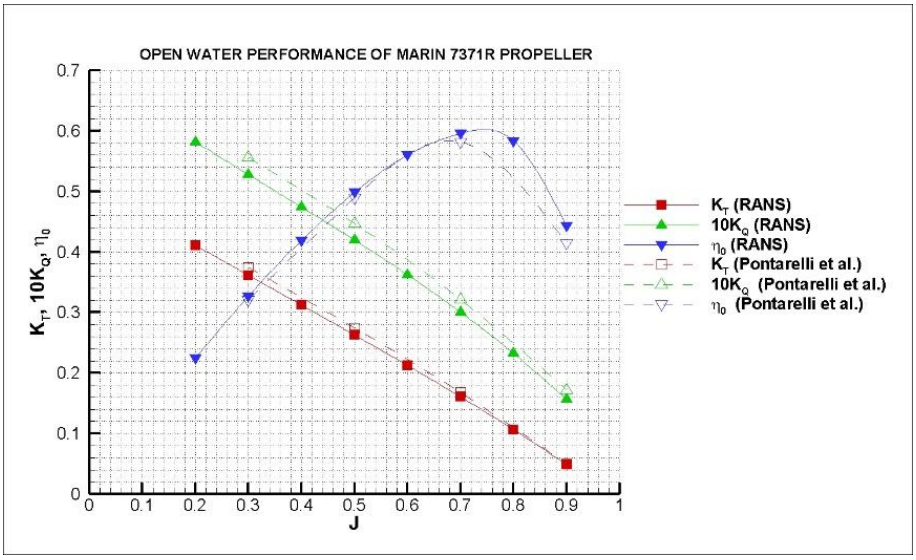

Fig. 6 Comparison of propeller open water curves

5.2 Submarine Total Resistance Analysis

The total resistance of the Joubert BB2 submarine model was calculated for a wide range of flow velocities numerically. The results were compared with a recent numerical study [19], in other words, the present study was validated numerically because there is no available experimental data in the open literature. The numerical results follow a similar trend with the other study as can be seen in Figure 7. These results belong to the model submarine in fully submerged conditions. The total resistance given in Figure 7 comprises frictional resistance and viscous pressure resistance. Both resistance components are generated inside the boundary layer. So, the difference between the two results in Figure 7 may be caused by the mesh structure near the submarine surface. The mesh density and the wall y^+ values affect the shear forces on the hull surface strongly.

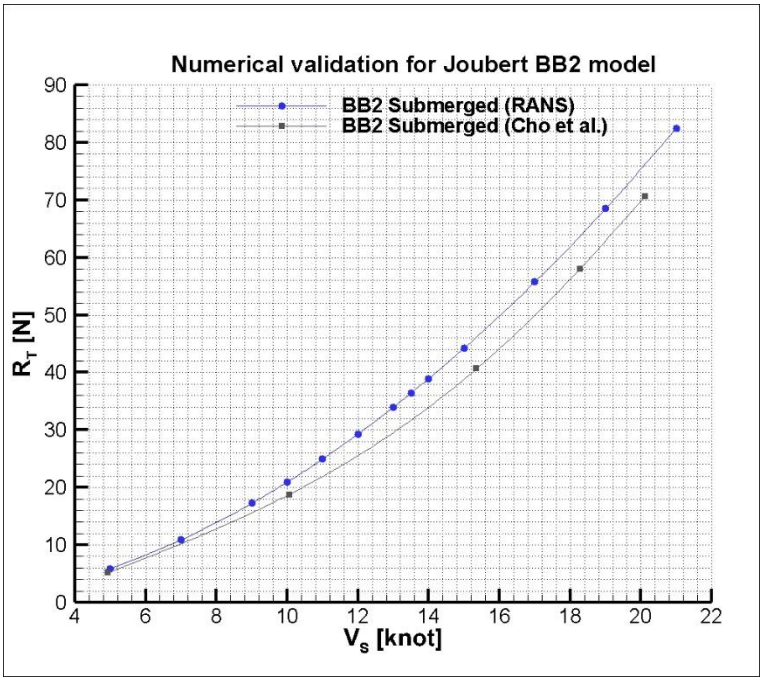

Fig. 7 Comparison with a similar numerical study

The total resistance data at various velocities is also used in the extrapolation to the full-scale total resistance. Hughes' 3D extrapolation method was used in the prediction of full-scale resistance performance. Following this method, the total resistance (R_T) was decomposed into three components; frictional resistance (R_F), viscous pressure resistance (R_{VP}) and wave-making resistance (R_W). In this case, the wave-making resistance is to be zero since the free surface effects are neglected in the fully submerged conditions.

$$R_T = R_F + R_{VP} + R_W \qquad R_W = 0 \tag{7}$$

$$1 + k = \frac{R_T}{R_F} \tag{8}$$

Here, k is the form factor of the submarine at each velocity. The link between the model and the full-scale submarine is maintained via the viscous pressure resistance and the frictional resistance is calculated using the ITTC 1957 correlation line [40].

$$C_F = \frac{0.075}{\left(log\left(Re\right) - 2\right)^2} \tag{9}$$

Here, the Reynolds number can be calculated as follows:

$$Re = \frac{VL}{\vartheta} \tag{10}$$

Figure 8 shows a comparison of two Joubert variants, BB1 and BB2. Joubert BB1 results are of the model experiments conducted at the towing tank while the 3-D model of BB1 is unavailable. BB2 results are of the present study based on RANS simulations. This comparison gives an idea about the difference between the two variants in terms of total resistance at fully submerged conditions. The BB1 model at the surface has higher total resistance due to the free surface effects as expected. On the other hand, the BB2 model, which is the latter design, has higher total resistance. BB2 model has longer tail fins which mean higher wetted surface area. This leads to higher frictional resistance. Note that, the frictional resistance is the dominant resistance component at fully submerged conditions because the free surface effects vanish.

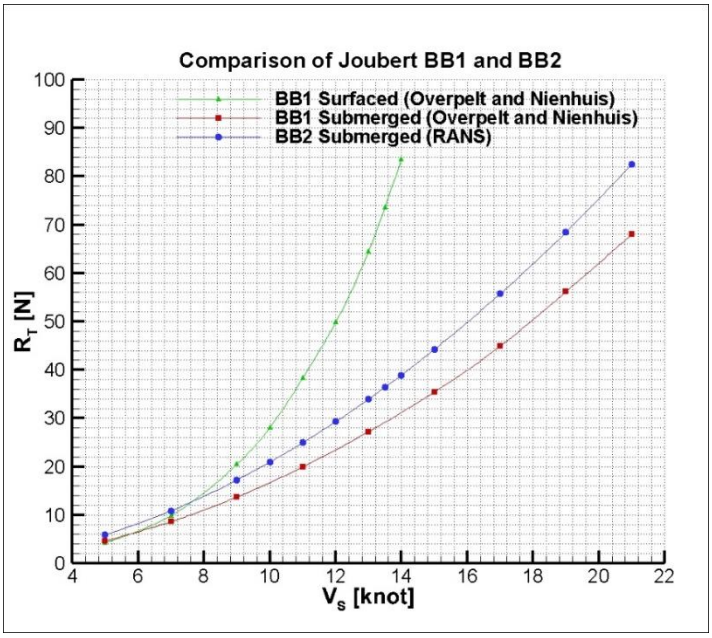

Fig. 8 Comparison of BB1 and BB2 models at different conditions

Full-scale RANS analyses were conducted to observe the scale effects on the total resistance. The full-scale CFD results were compared with the extrapolated full-scale results. The comparison was given in Figure 9. One may see that the full-scale CFD results are in good agreement with the extrapolated full-scale results having an average absolute relative error lower than 1%. Figure 9 shows that the appropriate extrapolation method for submerged bodies is the Hughes method which relies on the viscous pressure resistance. The full-scale resistance results were then used in the calculation of the thrust deduction factor. The full-scale resistance data was used as an input parameter in propulsion estimation with RANS and SPE methods.

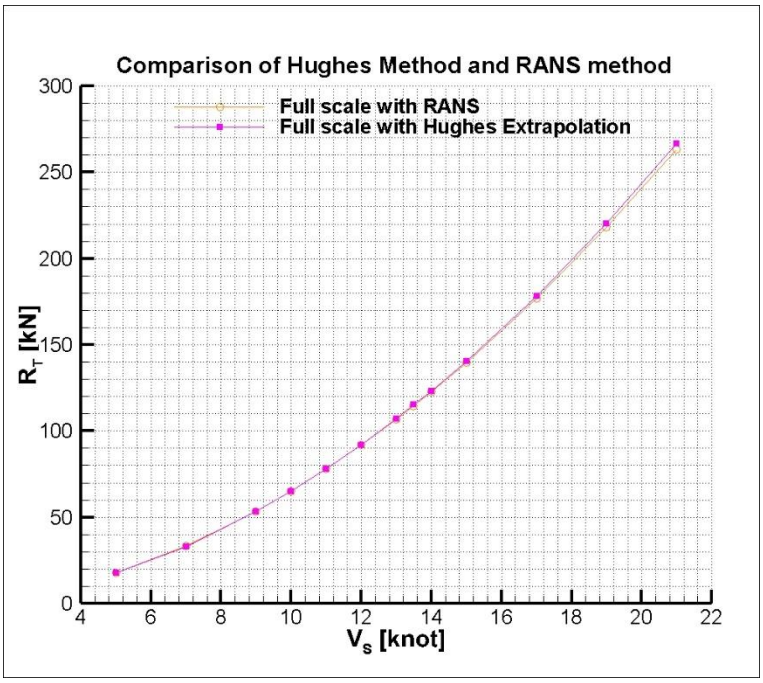

Fig. 9 Comparison of model extrapolated and full-scale CFD results

5.3 Flow field analysis of Joubert BB2 without propeller

Figure 10 shows the non-dimensional pressure distribution along the hull surface at 10 knots. The distribution was obtained on a horizontal plane cutting the center plane of the submarine, so the distribution does not represent the appendage effects. There is high pressure on the bow region that causes stagnation in the flow. The tail fins cause a pressure jump, however, negative pressure is observed on the stern region. The non-dimensional pressure coefficient is calculated by the following equation. The pressure distribution on the submarine hull for different scales were very similar to each other. This shows that the numerical model for both scales satisfy the dynamic similarity.

$$C_p = \frac{P_0 - P_\infty}{\rho . U_\infty^2} \tag{11}$$

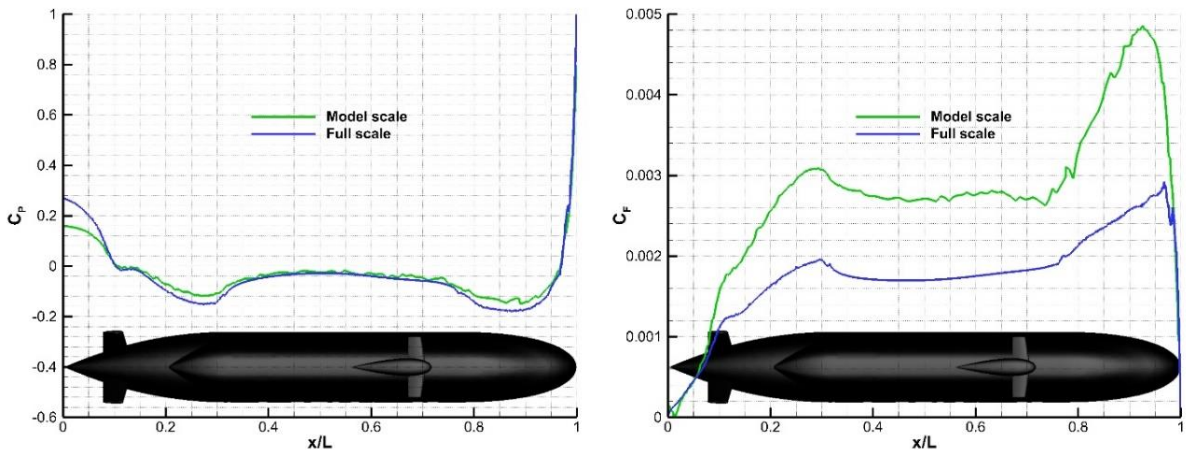

a) b)

Fig. 10 a) Non-dimensional pressure coefficient and b) skin friction coefficient distribution along the hull on the x-y plane

Figure 10 also shows the non-dimensional skin friction coefficient that represents the wall shear stress distribution on the submarine hull. The distribution was obtained on the same horizontal plane. The distribution reaches its peak at two endpoints of the submarine; bow and stern. The non-dimensional skin friction coefficient is calculated by the following equation.

$$C_f = \frac{\tau_w}{\rho . U_\infty^2} \tag{12}$$

The pressure distributions for both model and full scales are nearly the same as expected. There is a slight difference in the submarine stern. That is because the Reynolds numbers are different in these two scales. The boundary layer and the wake region differ with the scale factor.

6. Self-Propulsion Analyses

In this study, self-propulsion simulations were carried out in a RANSE-based CFD approach and obtained results were compared with the self-propulsion estimation (SPE) method; first mentioned in [3] and then validated with a free-running DTC Container Ship in [41]. It is considered appropriate to briefly explain the method in this section first. Then, comparisons with SPE are given in the following sub-sections in model and full scales.

SPE discretizes the ship-propeller interaction and considers the ship and the propeller as if they are single in the flow. Then, the method takes into account the interaction parameters to obtain the propulsion estimates of the ship. Four basic inputs are required for the method to generate results: the total resistance of the ship (R_T), the wake fraction (w), the thrust deduction factor (t) and the open-water propeller performance (K_T and K_Q curves with respect to J). Once these parameters are given as inputs to the method, SPE returns the propulsion estimates of the ship. Either the nominal or the effective wake fractions can be utilized in the method; however, [42] states that dramatic differences in the wake fraction may lead to inaccurate propulsion estimates. Implementation of nominal wake fraction implicitly assumes that the relative-rotative efficiency be equal to $\eta_R = 1$ [43]. In this paper, the nominal wake fraction is used in calculations with SPE. Results for the self-propulsion performance of the ship in model scale are given next. Then, necessary corrections advised by the ITTC are made and comparisons with RANSE-based results are provided.

The self-propulsion analyses for the submarine hull were conducted using the body force method. In this method, an actuator disc is created in the propeller plane with a constant diameter and thickness. This disc represents an infinite number of propeller blades and the hydrodynamic behavior of the propeller obtained from the open water analyses are defined in this region. Thus, the actuator disc and the model propeller have the same diameter and identical thrust distributions along the blade radius [44]. This method also provides convenience in modeling the hull-propeller interaction without modeling a discretized propeller behind the submarine.

With RANS analyses, the self-propulsion characteristics of Joubert BB2 were predicted in the model scale. The numerical analyses were carried out taking the friction deduction force (F_D) because the results were then extrapolated to the full scale. The equation F_D is derived from Bertram [45].

$$F_D = \frac{1}{2}\rho_M S_M V_M{}^2 \left(C_{FM} - C_{FS}\right) \tag{13}$$

Here, the subscript M stands for the model scale while S is full-scale. F_D is calculated as described in the ITTC guidelines [46–48]. In model scale analyses, it is considered that the sum of the propeller thrust force (T) and the friction deduction force (F_D) is equal to the total resistance (R_T) in the self-propelled case.

$$F_D + T = R_T \tag{14}$$

The equilibrium using equation 15 was obtained at the self-propulsion point of each velocity. At these points, the self-propulsion characteristics were calculated using the thrust identity method. This method was applied to the open water propeller curves obtained by CFD analyses (Chapter 5.1) and the relation between the advance coefficient and other non-dimensional coefficients were represented with second-order polynomials. Table 4 shows the detailed numerical results at the corresponding model velocities. The propulsive parameters in the table were calculated by the following equations.

$$t = \frac{T + F_D - R_T}{T} \tag{15}$$

Here, t is the thrust deduction factor while R_T is the total resistance calculated in bare hull analyses without the propeller. w is the effective wake fraction differing from the nominal wake fraction. It was calculated using the advance coefficient (J_T) obtained with the thrust identity method, the self-propulsion point (n) and the propeller diameter (D).

$$w = 1 - \frac{J_T n D}{V} \tag{16}$$

The open water propeller efficiency can be calculated as follows:

$$\eta_0 = \frac{T V_A}{2\pi n Q_0} \tag{17}$$

Here, Q_0 is the torque value obtained in the open water conditions. The relative rotative efficiency is calculated by the ratio of the open water torque to the torque calculated in the self-propelled case.

$$\eta_R = \frac{Q_0}{Q} \tag{18}$$

The hull efficiency is calculated by the ratio of the effective power to the thrust power.

$$\eta_H = \frac{P_E}{P_T} = \frac{R_T V}{T V_A} = \frac{1-t}{1-w} \tag{19}$$

The propulsive efficiency can then be expressed as follows:

$$\eta_D = \eta_H \eta_0 \eta_R \tag{20}$$

6.1 Self-Propulsion Characteristics by Model Scale CFD

Model scale self-propulsion results are given in this chapter. Model scale analyses were conducted taking the friction deduction force F_D into account. With this approach, the model scale results were then extrapolated to the full scale. The model scale results were compared and validated with the self-propulsion estimation (SPE) method since there are no experimental or numerical results in the model scale in the literature. In the SPE method, the wake fraction was chosen as the nominal wake fraction obtained in the resistance analyses and the thrust deduction factor was obtained from the self-propulsion analyses. The relation between nominal and effective wake fractions is given in Figure 11 while Table 5 gives the detailed data of RANS analyses at each submarine velocity.

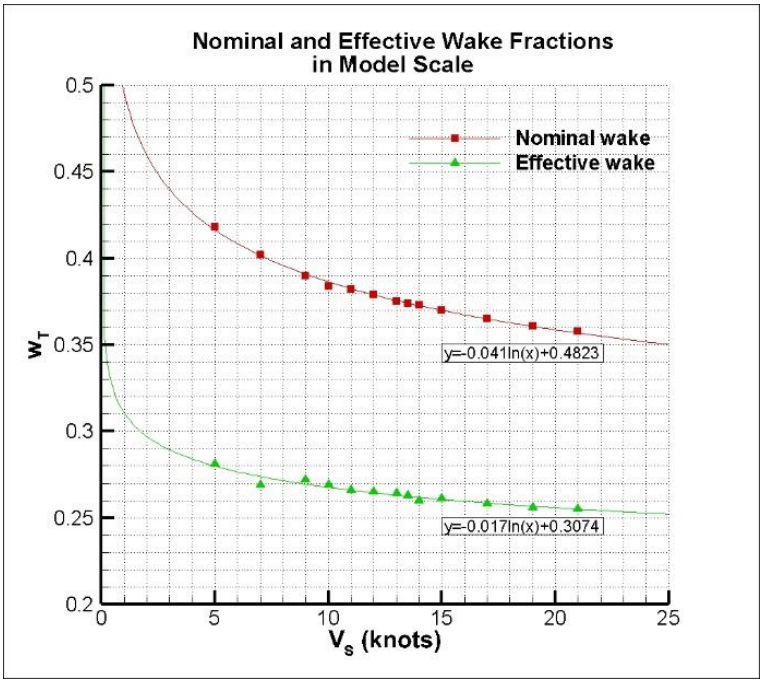

Fig. 11 Nominal and effective wake fractions in model scale

The nominal and effective wake fractions were calculated using the Taylor wake fraction equation (Equation 26). The effective wake fraction was calculated in self-propulsion analyses by obtaining the advance coefficient at the self-propulsion point. Both wake values show the logarithmic distribution (similar to [49]) in terms of submarine velocity as given in Figure 11. The effective wake values were calculated lower than the nominal wake values.

As can be seen in Table 4, each propulsive parameter shows a different trend with the velocity. The self-propulsion point increases with the increase in the velocity, in addition to this, the advance coefficient increases. The effective wake fraction, the thrust coefficient and the torque coefficient show a decrease while the velocity increases. The hull efficiency and other propulsive efficiencies do not follow a linear trend because the thrust deduction fluctuates with the velocity. The relative rotative efficiency does not change with the velocity while the open water propeller efficiency shows a very slight change.

Table 4 Self-propulsion characteristics obtained by model scale RANS method

V_m (m/s)	0.600	0.840	1.080	1.201	1.321	1.441	1.561	1.621	1.681	1.801	2.041	2.282	2.522
n(rps)	2.291	3.220	4.005	4.450	4.910	5.341	5.783	6.000	6.277	6.670	7.552	8.427	9.311
K_T	0.164	0.159	0.148	0.147	0.146	0.145	0.144	0.143	0.145	0.142	0.140	0.138	0.137
$10K_Q$	0.305	0.299	0.285	0.283	0.282	0.280	0.279	0.278	0.280	0.277	0.275	0.273	0.271
J	0.691	0.700	0.721	0.724	0.725	0.728	0.730	0.731	0.728	0.733	0.736	0.739	0.741
t	0.266	0.280	0.194	0.195	0.206	0.200	0.199	0.197	0.224	0.201	0.200	0.197	0.198
w_{eff}	0.281	0.269	0.272	0.269	0.266	0.265	0.264	0.263	0.260	0.261	0.258	0.256	0.255
η_H	1.021	0.986	1.107	1.101	1.082	1.089	1.087	1.089	1.049	1.081	1.079	1.080	1.076
η_0	0.593	0.594	0.597	0.597	0.597	0.598	0.598	0.598	0.598	0.598	0.598	0.598	0.597
η_R	0.995	0.995	0.995	0.996	0.996	0.996	0.996	0.996	0.996	0.996	0.996	0.996	0.996
η_D	0.602	0.583	0.658	0.655	0.644	0.648	0.647	0.648	0.624	0.643	0.642	0.642	0.641

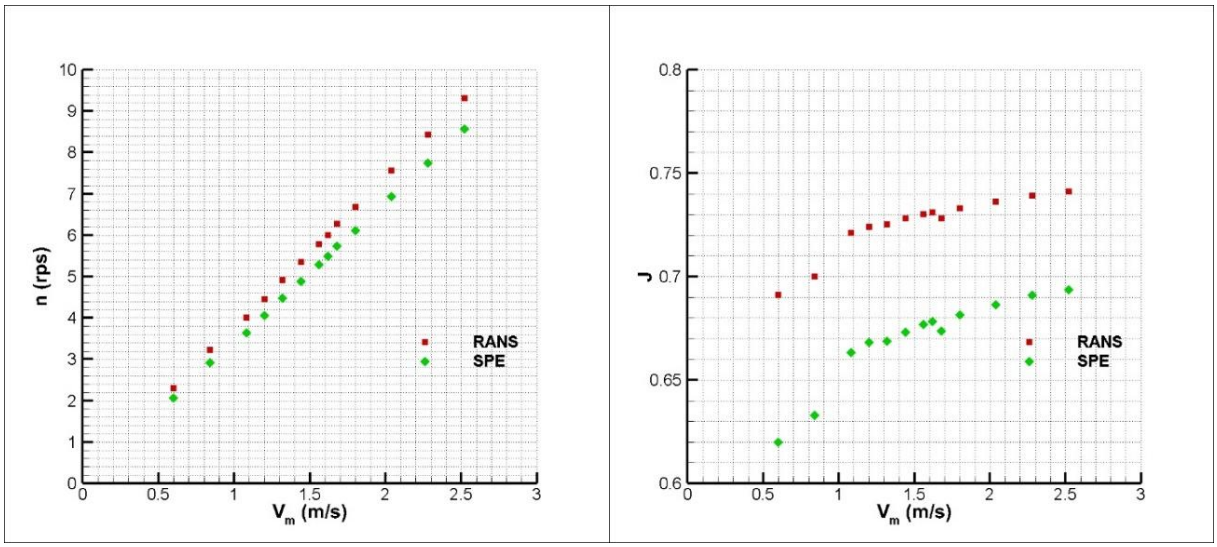

a) b)

Fig. 12 Validation with SPE method via a) self-propulsion point and b) advance coefficient in model scale

Figure 12 gives the results of the RANS and SPE methods. The self-propulsion points were in good agreement while there is some discrepancy in the advance coefficient. The difference in the advance coefficient is caused by the difference in the wake fraction. The self-propulsion point in the RANS method was obtained by using the effective wake fraction while the SPE method uses the nominal wake fraction. A higher wake fraction leads to a lower advance coefficient. Because the logic of the SPE method is based on the inputs without any need for propulsion analyses.

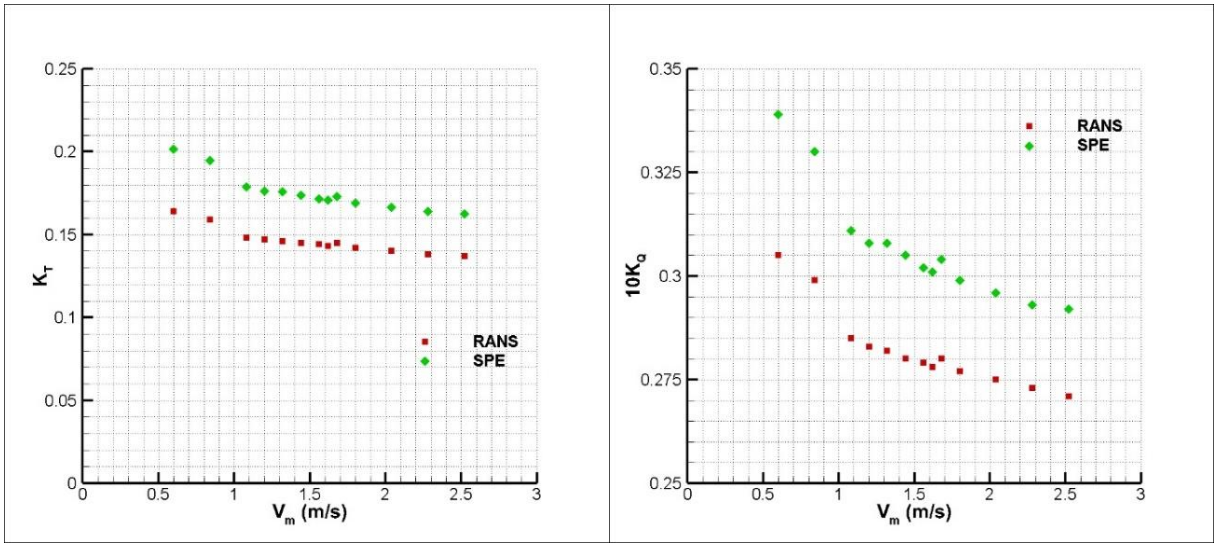

a) b)

Fig. 13 Validation with SPE method via a) thrust coefficient and b) torque coefficient in model scale

Figure 13 shows the comparison of these two methods (RANS and SPE) in terms of the thrust and torque coefficients. The same applies here to the difference between the methods. The use of different wake fractions makes the difference. A higher wake fraction leads to higher thrust and torque coefficients.

6.2 Extrapolation of Self-Propulsion Characteristics to Full-Scale by 1978 ITTC Method

To obtain the self-propulsion characteristics in full-scale, the total resistance has to be extrapolated to the full-scale following the ITTC recommendations. Here, the dynamic similarity was satisfied by keeping the Froude numbers of model and full-scale submarines equal. Froude similarity was maintained since the Reynolds similarity requires conducting the analyses in very high velocities. For submerged bodies, Froude similarity was used because of the need for high velocity in also similar studies [7,25,26].

The model scale self-propulsion characteristics were extrapolated to the full-scale for a better understanding of the submarine hydrodynamics. The extrapolation was made following the 1978 ITTC prediction method [47] at each submarine velocity. By this method, scale effect correction was made to predict the full-scale effective wake fraction. After, the full-scale results were compared with the other numerical results and the results of the self-propulsion estimation (SPE) method.

$$w_{TS} = (t + w_R) + (w_{TM} - t - w_R)\frac{(1+k)C_{FS} + \Delta C_F}{(1+k)C_{FM}} \tag{21}$$

Here, w_R is the rudder effect on the wake fraction which is recommended as 0.04 in the ITTC guideline. ΔC_F is the non-dimensional roughness effect and it was neglected in this study since the submarine surface is considered smooth. The propeller coefficients in full-scale (i.e. K_{TS}, $10K_{QS}$) were calculated using the thrust identity method by taking the full-scale corrections into account.

$$\frac{K_{TS}}{J_S^{\,2}} = \frac{1}{N_P}\frac{S_S}{2D_S^{\,2}}\frac{C_{TS}}{(1-t)(1-w_{TS})^2} \tag{22}$$

Here, N_P is the number of propellers which is 1 in this study. The propeller rotational speed was calculated by using the following equation:

$$n_S = \frac{(1-w_{TS})V_S}{J_{TS}D_S} \tag{23}$$

Other self-propulsion characteristics such as the efficiencies and power consumptions were calculated as described in the related guidelines [47,48].

$$P_E = R_{TS}V_S \tag{24}$$

$$P_D = 2\pi n_S Q_S \tag{25}$$

Here, P_E is the effective power while P_D is the delivered power. R_{TS} is the total resistance of the full-scale submarine and Q_S is the torque generated by the propeller in full-scale.

Table 5 presents the numerical results of the present study and other results based on the experiments and various CFD codes [11]. The results show that the full-scale results are in good agreement with other experimental/numerical results in terms of self-propulsion point. The self-propulsion analyses were extended to a wide range of submarine velocities and the full-scale results were obtained using the 1978 ITTC prediction method as it was validated at 10 knots. The full-scale CFD results for the same velocities were presented in Chapter 6.3 for a better discussion.

Table 5 Validation of the self-propulsion characteristics at 10 knots

	EFD	ReFRESCO/ PROCAL	ReFRESCO/ Discretized	REX/ Discretized	Full-scale extrapolation	Full-scale CFD	Full-scale SPE
$N(RPM)$	63.1	61.0	63.5	64.2	60.3	62.4	58.2
$1-t$	-	0.776	0.765	-	0.805	0.808	0.808
K_T	-	-	0.149	0.149	0.128	0.119	0.139
$10K_Q$	-	-	0.268	0.268	0.230	0.249	0.303

Figures 14-15 give an extended numerical validation with other results presented in [10,11]. The numerical results were compared with other numerical approaches based on different software for different submarine velocities in terms of self-propulsion point, propeller thrust coefficient and propeller torque coefficient. The results in the figures belong to the full-scale analyses while the results of the present study are the full-scale results extrapolated from the model scale. The self-propulsion estimation (SPE) method uses the open water curves, nominal wake fraction, thrust deduction factor and the full-scale extrapolated total resistance. Figure 14 shows the good agreement of the present results with other results. The discretized results as indicated in the figures are of the numerical approach using the body force method instead of modeling the propeller itself. The present study's results are found closer to the ones based on the discretized propeller. Within this comparison, one may see that the body force method in model scale gives similar results with the full-scale CFD method using the discretized propeller geometry. The relative difference increases with the increase in the submarine velocity. The extrapolation of the EFD result to the full-scale is not clear. The experimental results are available in terms of only the self-propulsion point. The present results show a better match with the experimental results which are extrapolated to the full-scale.

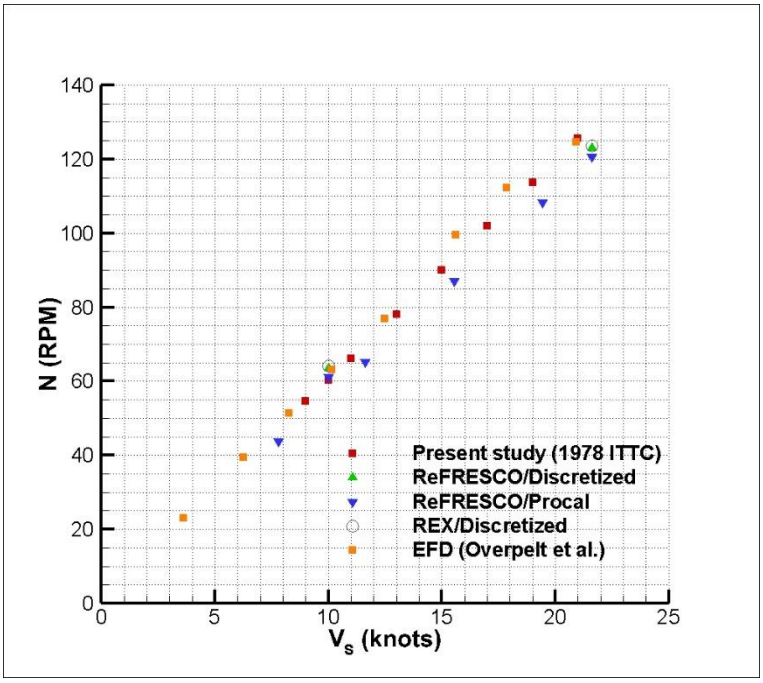

Fig. 14 Validation with other results via self-propulsion point in full-scale

Figure 15 shows the non-dimensional thrust coefficient of the propeller behind the submarine in the self-propelled case. The relative difference between the present results and other numerical results is due to the method used in modeling the rotating flow behind the ship. The results of the present study are lower than the other numerical results. The difference may be caused by the body force method and the extrapolation method applied using the thrust identity method. Note that the other numerical results are of the full-scale CFD results using the actual discretized propeller itself.

Figure 15 also shows the non-dimensional torque coefficient calculated by the thrust identity with the full-scale correction. Therefore, the relative difference is higher between the present results and the other results when compared with the thrust coefficient. The present study underestimates the torque coefficient at all submarine velocities, however, the trend is similar to the discretized propeller results.

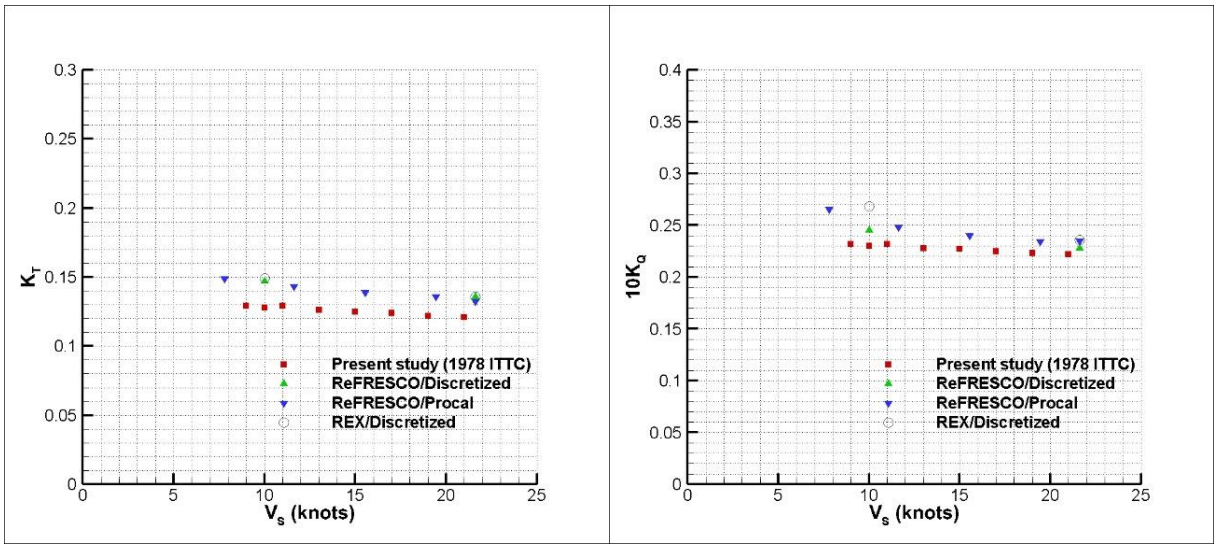

a) b)

Fig. 15 Validation with other results via a) thrust coefficient and b) torque coefficient in full-scale

Table 6 gives the self-propulsion characteristics of the Joubert BB2 submarine in full scale. The full-scale results were obtained with the extrapolation of the model scale results. However, the thrust deduction factor (t) was considered as same by neglecting the scale effects since there is not a correction procedure in ITTC guidelines [47,48]. There is a correlation between the propeller thrust, torque coefficients, advance coefficients and the submarine velocity following a linear trend. The relative rotative efficiency and the open water propeller efficiency do not change with the velocity. The propulsive efficiency nearly remains constant despite its trend in model scale. Most of the self-propulsion parameters are found independent of the submarine velocity.

Table 6 Self-propulsion characteristics obtained by 1978 ITTC prediction method

V_S (knots)	9	10	11	13	15	17	19	21
N(RPM)	54.7	60.32	66.20	78.15	90.01	101.89	113.78	125.63
K_T	0.129	0.128	0.129	0.126	0.125	0.124	0.122	0.121
$10K_Q$	0.232	0.230	0.232	0.228	0.227	0.225	0.223	0.222
J	0.763	0.765	0.763	0.768	0.771	0.773	0.776	0.778
t	0.194	0.195	0.206	0.199	0.201	0.200	0.197	0.198
w_{eff}	0.253	0.252	0.256	0.253	0.251	0.249	0.247	0.246
η_H	1.079	1.076	1.068	1.070	1.067	1.066	1.066	1.065
η_0	0.677	0.678	0.677	0.677	0.677	0.677	0.677	0.677
η_R	0.995	0.996	0.996	0.996	0.996	0.996	0.996	0.996
η_D	0.727	0.726	0.720	0.721	0.720	0.719	0.719	0.718

6.3 Self-Propulsion Characteristics by Full-Scale CFD

The propulsion analyses using the RANS method were carried out in full-scale to achieve the full-scale results by eliminating the possible scale effects. For the estimation of the propulsive parameters in full-scale, the equality of the total resistance and the thrust force was maintained at each velocity and the self-propulsion points were obtained. The full-scale RANS results were compared with the results of the 1978 ITTC prediction method and self-propulsion estimation (SPE) method. The results were also compared with the extrapolated experimental results in terms of the self-propulsion point.

Table 7 gives the propulsion characteristics of the Joubert BB2 submarine in full-scale. The results were obtained by conducting full-scale CFD to eliminate the scale effects and make a fair comparison with other methods applied in this study. The thrust deduction factor was directly calculated in full-scale. The scale effects on the thrust deduction factor can be seen by comparing the model and full scale results. The scale effects on the other parameters can also be observed.

Table 7 Self-propulsion characteristics obtained by full-scale RANS method

V_S (knots)	9	10	11	13	15	17	19	21
N(RPM)	56.22	62.40	68.52	80.70	93.00	105.12	117.42	129.48
K_T	0.120	0.119	0.118	0.116	0.115	0.114	0.113	0.112
$10K_Q$	0.250	0.249	0.247	0.245	0.243	0.241	0.240	0.239
t	0.189	0.192	0.191	0.188	0.191	0.188	0.191	0.194

The detailed comparison of the full-scale CFD, 1978 ITTC method, full-scale SPE method and the experimental results can be seen in Figure 16. Here, the 1978 ITTC is the extrapolated model scale results using the thrust identity method while full-scale SPE is the one based on full-scale total resistance, thrust deduction factor and nominal wake fraction. The results are close to each other while the SPE method underestimates the self-propulsion point at all velocities. The difference between the full-scale RANS and extrapolated results increases with the velocity. This means that the effects of the scale and full-scale corrections of the prediction method become more important at high velocities.

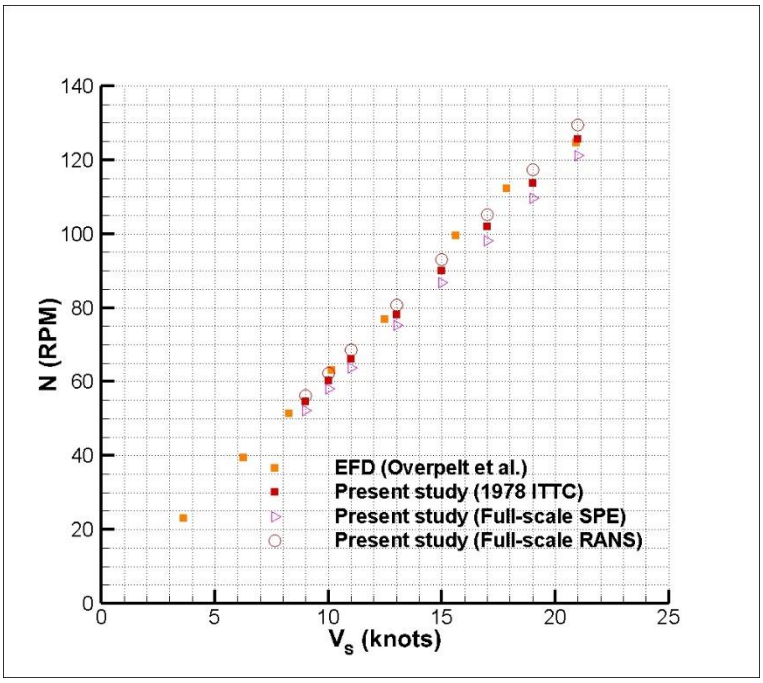

Fig. 16 Comparison of full-scale RANS with other methods

The nominal wake fraction was calculated using Equation (26) based on Taylor's wake fraction. Figure 17 gives the average nominal wake fractions on the propeller plane located behind the submarine in the model and full scales. It is observed that there is a logarithmic relation between the submarine velocity and the nominal wake fraction. The nominal wake fraction shows a decrease with the increase in the submarine velocity. The scale effects were observed very strongly that the nominal wake fraction was calculated higher in the model scale at all velocities. The difference between the model and full-scale wake fractions decreases with the increase in the submarine velocity.

$$w_n = \frac{V_S - V_A}{V_S} \tag{26}$$

Here, is the submarine velocity and is the average advance velocity in the axial direction at the propeller plane. The nominal wake fractions are one of the input parameters in the self-propulsion estimation (SPE) method to obtain the propulsion characteristics in both model and full scales.

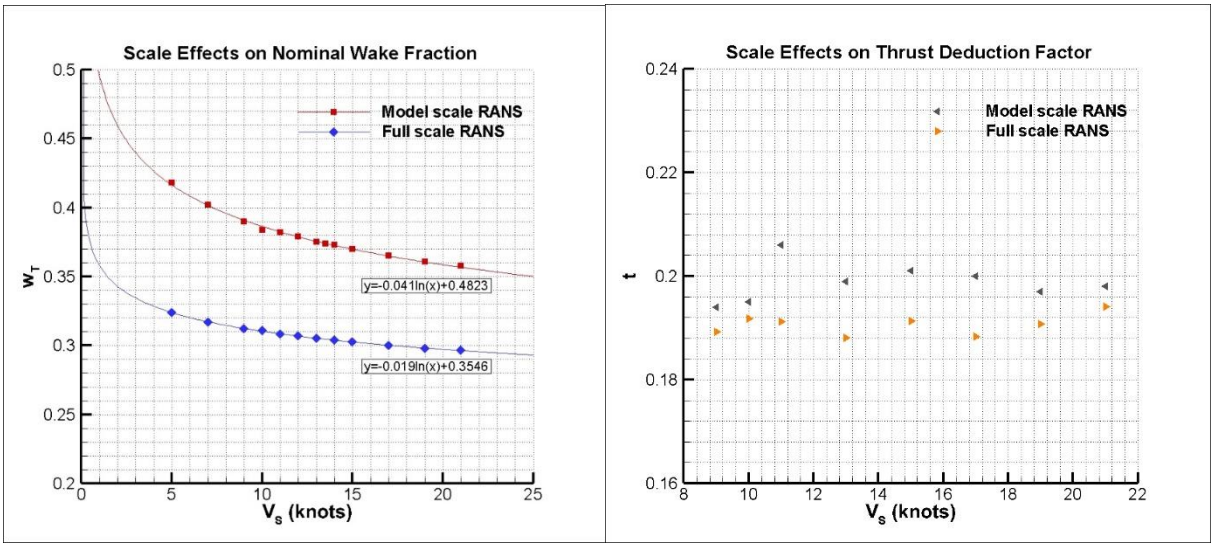

Fig. 17 Scale effects on the nominal wake fraction and thrust deduction factors

The thrust deduction factor was calculated using Equation (15) in model scale self-propulsion analyses. The same factor in full-scale was calculated similarly but also eliminating the friction deduction force. Figure 17 shows that the flow behind the submarine without propeller is more vulnerable to the scale effects than the self-propelled case. The nominal wake fraction is highly affected from the scale factor while the relative difference is lower in thrust deduction factor.

7. Discussion

Ship-propeller interaction plays a significant role in ship propulsion. Determination of bare hull resistance and open-water propeller performance might give an idea about a ship's propulsion performance; however, a robust prediction method should also cover the interaction between the two. A ship changes the flow velocity received by the propeller while the propeller changes the total resistance of the ship. We can assemble all the effects of the former by the wake fraction and the thrust deduction factor for the latter.

On the other hand, the self-propulsion case of a ship can be simulated by RANS-based CFD. This method eliminates all the needs for a preliminary study that includes obtaining bare hull resistance or open-water propeller performance etc. Although CFD offers a very practical way of going directly to the solution, it is only valid for one single case. To understand the whole propulsion mechanism of the ship in a range of velocities, one needs to conduct many CFD simulations.

To avoid doing so, methods of propulsion estimation (such as SPE used in this study, the thrust identity, the torque identity, etc.) are used. Once validated with experiments or numerical simulations, these methods can quickly reveal the whole propulsion performance of the ship. However, the estimation methods heavily rely on interaction parameters: a correct estimate of the thrust deduction factor and the wake fraction should be available for accurate results.

The present study is focused on numerical analyses based on the RANS method. RANS analyses were conducted using an actuator disc and implementing the body force method similar to the studies of [50] and [51]. RANS results were compared with the self-propulsion estimation (SPE) method in terms of propulsive parameters such as the advance coefficient, thrust/torque coefficients and the self-propulsion point. In the SPE method, total resistance, nominal wake fraction and thrust deduction factor, obtained from the model scale, RANS analyses were employed. In the calculation of the RANS-based propulsive parameters, the effective wake fraction obtained from the propulsion analyses was used. This leads to some

discrepancy in terms of the propeller non-dimensional coefficients ($J, K_T, 10K_Q$) while the self-propulsion points were close in both methods. The same happens for the full-scale results. The full-scale propulsive parameters based on the model scale RANS analyses were obtained using the extrapolation method. The extrapolation was made with the 1978 ITTC performance prediction method and the thrust identity approach was employed similar to the study of [52].

Full-scale RANS analyses were carried out similar to the model scale cases. Total resistance and nominal wake fraction parameters were used as input to the full-scale SPE estimation. For the open water curves, the full-scale corrections recommended by ITTC were applied. The thrust deduction factor was obtained from the full-scale propulsion analyses and used in the SPE calculations.

8. Conclusion

This study presents a comprehensive total resistance, wake fraction and propulsion data of Joubert BB2 with MARIN7371R propeller both in model scale and full scale. Consequently, the CFD method for the submarine hydrodynamics in model scale coupled with the body force method can be used in the performance prediction of submerged bodies. Compared to the discretized propeller approach, it will provide a faster and simpler solution.

A commercial CFD solver was employed and Joubert BB2 with MARIN7371R propeller was modeled in multiple scales. Total resistance, nominal wake fraction, propulsion characteristics were predicted numerically in model scale and compared with the self-propulsion estimation (SPE) method. The model scale results were then extrapolated to the full-scale for a more realistic estimation using the 1978 ITTC performance prediction method. Finally, full-scale RANS analyses were conducted to estimate the full-scale performance directly and to observe the scale effects on the resistance and propulsion characteristics. A comprehensive self-propulsion performance prediction was presented for a wide range of submarine velocities in full scale. Within this framework, some findings were described below:

• Numerical simulations conducted in multiple ship scales showed that the scale effects on the nominal wake fraction is higher than the thrust deduction factor.

• The logarithmic relation between the submarine velocity and the wake fraction was observed in the model scale for both nominal and effective wake fractions. This relation is disrupted in full-scale following the full-scale correction as recommended in the 1978 ITTC performance prediction method.

• Numerical results obtained in the present study were in good agreement with other numerical results in terms of total resistance. The open-water propeller performance was good in good accordance with the experimental results. The full-scale total resistance showed that the Hughes' extrapolation method is appropriate for submerged vessels.

• The numerically obtained propulsion characteristics were compared with the available numerical and experimental results. The present study was in good agreement with other full-scale CFD studies. The model and full-scale results of the propulsion case were compared with the self-propulsion estimation (SPE) method and the results were found to be satisfactory.

• The results show that the SPE method can be utilized in the estimation of propulsive characteristics. The input parameters in this study were obtained from the RANS analyses. However, several empirical methods can also be employed to predict these parameters e.g. total resistance, nominal wake fraction and thrust deduction factors.

With regard to this study, free surface effects on the propulsion characteristics can be investigated in multiple scales using RANS method and SPE method as a further research. In

addition, a sensitivity analysis can be conducted about the propulsive parameters using SPE method in multiple scales.

Acknowledgements

The author wishes to thank Maritime Research Institute Netherlands (MARIN) for providing the submarine and propeller geometry. The author also thanks Yıldız Technical University for the support in the usage of the commercial CFD software and Mr. Burak Aydogdu for his support throughout this study.

REFERENCES

[1] Chase, N., 2012. Simulations of the DARPA Suboff Submarine Including Self-Propulsion with the E1619 Propeller. Master Thesis, *University of Iowa*.

[2] Chase, N., Carrica, P. M., 2013. Submarine Propeller Computations and Application to Self-Propulsion of DARPA Suboff. *Ocean Engineering*, 60, 68–80. https://doi.org/10.1016/j.oceaneng.2012.12.029

[3] Kinaci, O. K., Gokce, M. K., Alkan, A. D., Kukner, A., 2018. On Self-Propulsion Assessment of Marine Vehicles. *Brodogradnja: Teorija i praksa brodogradnje i pomorske tehnike*, 69(4), 29–51. https://doi.org/10.21278/brod69403

[4] Posa, A., and Balaras, E., 2018. Large-Eddy Simulations of a Notional Submarine in Towed and Self-Propelled Configurations. *Computers & Fluids*, 165, 116–126. https://doi.org/10.1016/j.compfluid.2018.01.013

[5] Özden, Y. A., Özden, M. C., Demir, E., Kurdoğlu, S., 2019. Experimental and Numerical Investigation of DARPA Suboff Submarine Propelled with INSEAN E1619 Propeller for Self-Propulsion. *Journal of Ship Research*, 63(04), 235–250. https://doi.org/10.5957/JOSR.09180084

[6] Wang, L., Martin, J. E., Felli, M., Carrica, P. M., 2020. Experiments and CFD for the Propeller Wake of a Generic Submarine Operating near the Surface. *Ocean Engineering*, 206, 107304. https://doi.org/10.1016/j.oceaneng.2020.107304

[7] Sezen, S., Delen, C., Dogrul, A., Atlar, M., 2021. An Investigation of Scale Effects on the Self-Propulsion Characteristics of a Submarine. *Applied Ocean Research*, 113, 102728. https://doi.org/10.1016/j.apor.2021.102728

[8] Overpelt, B., Nienhuis, B., 2014. Bow Shape Design for Increased Surface Performance Of An SSK Submarine. *Warship 2014: Naval Submarines & UUVs*, Bath, UK. https://doi.org/10.3940/rina.ws.2014.04

[9] Toxopeus, S., Kuin, R., Kerkvliet, M., Hoeijmakers, H., Nienhuis, B., 2014. Improvement of Resistance and Wake Field of an Underwater Vehicle by Optimising the Fin-Body Junction Flow With CFD. *ASME 2014 33rd International Conference on Ocean, Offshore and Arctic Engineering*, San Francisco, California, USA. https://doi.org/10.1115/OMAE2014-23784

[10] Overpelt, B., Nienhuis, B., Anderson, B., 2015. Free Running Manoeuvring Model Tests On A Modern Generic SSK Class Submarine (BB2). *Pacific International Maritime Conference*, Sydney, Australia.

[11] Carrica, P. M., Kerkvliet, M., Quadvlieg, F., Pontarelli, M., Martin, J. E., 2016. CFD Simulations and Experiments of a Maneuvering Generic Submarine and Prognosis for Simulation of Near Surface Operation. *31st Symposium on Naval Hydrodynamics*, Monterey, California, USA.

[12] Hally, D., 2017. A RANS-BEM Coupling Procedure for Calculating the Effective Wakes of Ships and Submarines. *5th International Symposium on Marine Propulsion*, Espoo, Finland.

[13] Pontarelli, M., 2017. Flow Regimes and Instabilities of Propeller Crashback. MSc Thesis, *University of Iowa*.

[14] Pontarelli, M., Martin, J. E., Carrica, P. M., 2017. Dynamic Instabilities in Propeller Crashback. *5th International Symposium on Marine Propulsion*, Espoo, Finland.

[15] Kim, H., 2017. Six-DOF Motion Response and Manoeuvring Simulation of an Underwater Vehicle. PhD Thesis, *University of Tasmania*.

[16] Kim, H., Leong, Z. Q., Ranmuthugala, D., Clarke, D., Binns, J., Duffy, J., 2018. Numerical Investigation into the Effect of Incidence Flow Angles on Submarine Propeller Hydrodynamic Characteristics. *21st Australasian Fluid Mechanics Conference*, Adelaide, Australia.

[17] Carrica, P. M., Kim, Y., Martin, J. E., 2019. Near-Surface Self Propulsion of a Generic Submarine in Calm Water and Waves. *Ocean Engineering*, 183, 87–105. https://doi.org/10.1016/j.oceaneng.2019.04.082

[18] Carrica, P. M., Kim, Y., Martin, J. E., 2020. Vertical Zigzag Maneuver of a Generic Submarine. *Ocean Engineering*, 219, 108386. https://doi.org/10.1016/j.oceaneng.2020.108386

[19] Cho, Y. J., Seok, W., Cheon, K.-H., Rhee, S. H., 2020. Maneuvering Simulation of an X-Plane Submarine Using Computational Fluid Dynamics. *International Journal of Naval Architecture and Ocean Engineering*, 12, 843–855. https://doi.org/10.1016/j.ijnaoe.2020.10.001

[20] Joubert, P. N., 2004. Some Aspects of Submarine Design Part 1. Hydrodynamics. DSTO-TR-1622, *Australia Defence Science and Technology Organisation*.

[21] Joubert, P. N., 2006. Some Aspects of Submarine Design Part 2. Shape of a Submarine 2026. DSTO-TR-1920, *Australia Defence Science and Technology Organisation*.

[22] Wilcox, D. C., 2006. Turbulence Modeling for CFD. *DCW Industries*. La Cãnada, California, USA.

[23] Wilcox, D. C., 2008. Formulation of the k-w Turbulence Model Revisited. *AIAA Journal*, 46(11), 2823–2838. https://doi.org/10.2514/1.36541

[24] ITTC, 2014. 7.5-03-02-03 Practical Guidelines for Ship CFD Applications. *ITTC - Recommended Procedures and Guidelines*.

[25] Uzun, D., Sezen, S., Ozyurt, R., Atlar, M., Turan, O., 2021. A CFD Study: Influence of Biofouling on a Full-Scale Submarine. *Applied Ocean Research*, 109, 102561. https://doi.org/10.1016/j.apor.2021.102561

[26] Uzun, D., Sezen, S., Atlar, M., Turan, O., 2021. Effect of Biofouling Roughness on the Full-Scale Powering Performance of a Submarine. *Ocean Engineering*, 238, 109773. https://doi.org/10.1016/j.oceaneng.2021.109773

[27] Argyropoulos, C. D., Markatos, N. C., 2015. Recent Advances on the Numerical Modelling of Turbulent Flows. *Applied Mathematical Modelling*, 39(2), 693–732. https://doi.org/10.1016/j.apm.2014.07.001

[28] Menter, F. R., 1994. Two-Equation Eddy-Viscosity Turbulence Models for Engineering Applications. *AIAA Journal*, 32(8), 1598–1605. https://doi.org/10.2514/3.12149

[29] Menter, F. R., 2009. Review of the Shear-Stress Transport Turbulence Model Experience from an Industrial Perspective. *International Journal of Computational Fluid Dynamics*, 23(4), 305–316. https://doi.org/10.1080/10618560902773387

[30] Moussa, K., 2014. Computational Modeling of Propeller Noise: NASA SR-7A Propeller. MSc Thesis, University of Waterloo.

[31] Song, S., Demirel, Y. K., Atlar, M., 2019. An Investigation Into the Effect of Biofouling on Full-Scale Propeller Performance Using CFD. *ASME 2019 38th International Conference on Ocean, Offshore and Arctic Engineering*, Glasgow, Scotland, UK. https://doi.org/10.1115/OMAE2019-95315

[32] Celik, I. B., Ghia, U., Roache, P. J., Freitas, C. J., Raad, P. E., 2008. Procedure for Estimation and Reporting of Uncertainty Due to Discretization in CFD Applications. *Journal of Fluids Engineering*, 130(7), 078001. https://doi.org/10.1115/1.2960953

[33] Xing, T., Stern, F., 2010. Factors of Safety for Richardson Extrapolation. *Journal of Fluids Engineering*, 132(6), 061403. https://doi.org/10.1115/1.4001771

[34] Owen, D., Demirel, Y. K., Oguz, E., Tezdogan, T., Incecik, A., 2018. Investigating the Effect of Biofouling on Propeller Characteristics Using CFD. *Ocean Engineering*, 159, 505–516. https://doi.org/10.1016/j.oceaneng.2018.01.087

[35] Sezen, S., Dogrul, A., Delen, C., Bal, S., 2018. Investigation of Self-Propulsion of DARPA Suboff by RANS Method. *Ocean Engineering*, 150, 258–271. https://doi.org/10.1016/j.oceaneng.2017.12.051

[36] Song, S., Demirel, Y. K., Atlar, M., 2020. Penalty of Hull and Propeller Fouling on Ship Self-Propulsion Performance. *Applied Ocean Research*, 94, 102006. https://doi.org/10.1016/j.apor.2019.102006

[37] ITTC, 2014. 7.5-03-01-01 Uncertainty Analysis in CFD, Verification and Validation Methodology and Procedures. *ITTC - Recommended Procedures and Guidelines*.

[38] Cosner, R., Oberkampf, B., Rumsey, C., Rahaim, C., Shih, T., 2006. AIAA Committee on Standards for Computational Fluid Dynamics: Status and Plans. *44th AIAA Aerospace Sciences Meeting and Exhibit*, Reno, Nevada, USA. https://doi.org/10.2514/6.2006-889

[39] Stern, F., Wilson, R. V., Coleman, H. W., Paterson, E. G., 2001. Comprehensive Approach to Verification and Validation of CFD Simulations—Part 1: Methodology and Procedures. *Journal of Fluids Engineering*, 123(4), 793–802. https://doi.org/10.1115/1.1412235

[40] ITTC, 1957. Report of Resistance Committee. Madrid, Spain.

[41] Kinaci, O. K., Delen, C., Bitirgen, R., Bayezit, A., Bayezit, I., Ozturk, D., Gunguder, B., 2021. Free-Running Tests for DTC Self-Propulsion – An Investigation of Lateral Forces Due to the Rudder and the Propeller. *Applied Ocean Research*, 116, 102877. https://doi.org/10.1016/j.apor.2021.102877

[42] Gokce, M. K., Kinaci, O. K., Alkan, A. D., 2019. Self-Propulsion Estimations for a Bulk Carrier. *Ships and Offshore* Structures, 14(7), 656–663. https://doi.org/10.1080/17445302.2018.1544108

[43] Kinaci, O. K., Gokce, M. K., Delen, C., 2020. Resistance Experiments and Self-Propulsion Estimations of Duisburg Test Case at 1/100 Scale. *Ship Technology Research*, 67(2), 109–120. https://doi.org/10.1080/09377255.2020.1729454

[44] Krasilnikov, V., 2013. Self-Propulsion RANS Computations with a Single-Screw Container Ship. *3rd International Symposium on Marine Propulsors*, Tasmania, Australia.

[45] Bertram, V., 2014, Practical Ship Hydrodynamics, *Elsevier Science*.

[46] ITTC, 2017. Report of Propulsion Committee. Wuxi, China

[47] ITTC, 2017. 7.5-02-03-01.4 1978 ITTC Performance Prediction Method. *ITTC - Recommended Procedures and Guidelines*.

[48] ITTC, 2017. 7.5-02-03-01.1 Propulsion/Bollard Pull Test. *ITTC - Recommended Procedures and Guidelines*.

[49] Can, U., Delen, C., Bal, S., 2020. Effective Wake Estimation of KCS Hull at Full-Scale by GEOSIM Method Based on CFD. *Ocean Engineering*, 218, 108052. https://doi.org/10.1016/j.oceaneng.2020.108052

[50] Jasak, H., Vukčević, V., Gatin, I., Lalović, I., 2019. CFD Validation and Grid Sensitivity Studies of Full Scale Ship Self Propulsion. I*nternational Journal of Naval Architecture and Ocean Engineering*, 11(1), 33–43. https://doi.org/10.1016/j.ijnaoe.2017.12.004

[51] Villa, D., Gaggero, S., Gaggero, T., Tani, G., Vernengo, G., Viviani, M., 2019. An Efficient and Robust Approach to Predict Ship Self-Propulsion Coefficients. *Applied Ocean Research*, 92, 101862. https://doi.org/10.1016/j.apor.2019.101862

[52] Gaggero, S., Villa, D., Viviani, M., 2017. An Extensive Analysis of Numerical Ship Self-Propulsion Prediction via a Coupled BEM/RANS Approach. *Applied Ocean Research*, 66, 55–78. https://doi.org/10.1016/j.apor.2017.05.005

Submitted: 16.03.2022.
Accepted: 11.04.2022.

Ali Dogrul
Department of Naval Architecture and Marine Engineering, Turkish Naval Academy, National Defense University, 34940, Istanbul, Türkiye
adogrul@dho.edu.tr (ORCID: 0000-0003-3236-555X)